

Numerical studies on non-shear and shear flows past a 5:1 rectangular cylinder

Qiang Zhou, Shuyang Cao* and Zhiyong Zhou

State Key Laboratory for Disaster Reduction in Civil Engineering, Tongji University,
Shanghai 200092, P. R. China

(Received August 1, 2012, Revised December 26, 2012, Accepted January 4, 2013)

Abstract. Large Eddy Simulations (LES) were carried out to investigate the aerodynamic characteristics of a rectangular cylinder with side ratio $B/D=5$ at Reynolds number $Re=22,000$ (based on cylinder thickness). Particular attention was devoted to the effects of velocity shear in the oncoming flow. Time-averaged and unsteady flow patterns around the cylinder were studied to enhance understanding of the effects of velocity shear. The simulation results showed that the Strouhal number has no significant variation with oncoming velocity shear, while the peak fluctuation frequency of the drag coefficient becomes identical to that of the lift coefficient with increase in velocity shear. The intermittently-reattached flow that features the aerodynamics of the 5:1 rectangular cylinder in non-shear flow becomes more stably reattached on the high-velocity side, and more stably separated on the low-velocity side. Both the mean and fluctuating drag coefficients increase slightly with increase in velocity shear. The mean and fluctuating lift and moment coefficients increase almost linearly with velocity shear. Lift force acts from the high-velocity side to the low-velocity side, which is similar to that of a circular cylinder but opposite to that of a square cylinder under the same oncoming shear flow.

Keywords: rectangular cylinder; shear parameter; large eddy simulation; aerodynamic forces; vortex shedding; flow reattachment

1. Introduction

Rectangular cylinders are common configurations in many structures, such as bridges, tall buildings and so on. Thus, the flow past a bluff body with a rectangular cross section is of direct relevance to structural problems, and wind-induced vibration is one of the most important issues.

The majority of studies on flow around a rectangular cylinder have been conducted under uniform oncoming flow conditions, in which vortices with equal strength alternately shed from each side of the cylinder. However, in many practical applications, a cylindrical structure is immersed in a non-uniform flow. A bridge deck in the atmospheric boundary layer is an example, in which the vertical mean wind profile is one factor in determining the wind load on it. The influence of velocity profile or velocity shear in the oncoming flow becomes more significant in non-synoptic wind like a downburst, where wind speed increases rapidly near the ground and reaches its maximum at a height of about 80-100 m, and then decreases with height resulting in a

*Corresponding author, Professor, E-mail: shuyang@tongji.edu.cn

stronger velocity shear than in synoptic winds. Strong velocity shear can also be created in complex topography. Therefore, the variation of aerodynamic behaviors of a rectangular cylinder with velocity shear needs to be studied in detail. In this study, a dimensionless shear parameter $\beta = G \times D / U_C = (dU / dy) \times (D / U_C)$ is defined to express the extent of velocity shear, where U_C is the mean velocity at the center plane, D is the thickness of the rectangular cylinder and G is the velocity gradient, as illustrated in Fig. 1. The magnitude of the shear parameter expresses the velocity difference between the upper and lower surfaces of the rectangular cylinder.

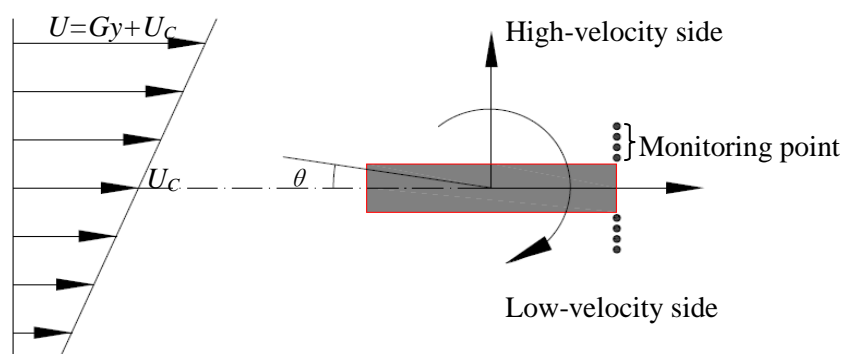


Fig. 1 Schematic of shear flow configuration

There have been a few published papers on shear flow past bluff bodies. Kiyama *et al.* (1980) investigated vortex shedding from a circular cylinder in shear flow and reported that the critical Reynolds number for the occurrence of vortex shedding is larger than in non-shear flow. Kiyama's work was followed by studies on circular cylinders (e.g., Sumner and Akosile 2003, Cao *et al.* 2010), and on square cylinders (e.g., Cao *et al.* 2012). However, the common points of interest of these investigations were how the Strouhal number varies with shear parameter and Reynolds number. Little attention was devoted to shear effects on aerodynamic forces and the underlying background. In addition, there has been no other reported study on shear effects on a rectangular cylinder, except for the experimental study of Onirsuka *et al.* (2000). The insufficient study of shear effects over a rectangular cylinder partly motivated the present study.

The work described in this paper investigated the aerodynamic characteristics of a rectangular cylinder with side ratio $B/D=5$ in non-shear and shear flows at $Re=22,000$, where the Reynolds number Re is based on the thickness of the rectangular cylinder D and the centerline velocity U_C . Particular attention was devoted to the effects of velocity shear in the oncoming flow. The side ratio 5:1 was chosen as the study objective because it has often been adopted as a reference for investigations of the aerodynamics and aeroelasticity of a bridge deck and other structural members (Matsumoto 1996). In addition, a $B/D=5$ rectangular cylinder has very delicate dynamic behaviors of vortex shedding characterized by massive flow separation due to the sharp leading edges and intermittent reattachment on side surfaces forming unsteady separating bubbles, which merits study from the viewpoint of fundamental bluff body aerodynamics. The aerodynamic behavior of a fixed sharp-edged rectangular cylinder with $B/D=5$ in non-shear flow has been widely investigated (Le *et al.* 2009). Under the framework of Benchmark on the Aerodynamics of a Rectangular

Cylinder (BARC) that was launched in July 2008 (Bartoli *et al.* 2008), systematic research has been carried out, aimed at providing a contribution to the analysis of turbulent, separated flow around a rectangular cylinder with $B/D=5$ with informative achievements (e.g., Schewe 2009, Bruno *et al.* 2010, 2012, Mannini *et al.* 2010, 2011, Bartoli *et al.* 2011, Ribeiro 2011, Bronkhorst *et al.* 2011).

With the occurrence of shear parameter, i.e., an asymmetry in the oncoming flow, the separated flows on the two sides of the rectangular cylinder must differ, resulting in aerodynamic behaviors different with those in non-shear flow. Non-zero-mean lift and moment forces, which are important factors in determining the behavior of flow-structure coupling, must appear. However, till now there has been no reported research on the flow around a 5:1 rectangular cylinder in shear flows. Onitsuka *et al.* (2000) studied experimentally the Strouhal number of rectangular cylinders in linear shear flows at $Re=3.2-9.7 \times 10^4$ when $B/D=0.2-3$. However, the separated shear layers did not reattach to the side surface in the range of $B/D=0.2-3$. The side ratio $B/D=5$ considered in this study involves intermittent flow reattachment, which makes the flow more sensitive to the asymmetry in the oncoming flow.

In this study, we investigated the vortex shedding and aerodynamic forces on a 5:1 rectangular cylinder in both non-shear and shear flows by Large Eddy Simulation (LES) using a Smagorinsky subgrid model (1963). We employed a structured grid mesh system for finite volume approximation of incompressible Navier-Stokes equations. The FLUENT® package was used as a solver of the governing equations, but the options offered by FLUENT® for simulation were carefully selected in order to achieve reliable results. The aerodynamic characteristics of the 5:1 rectangular cylinder in non-shear flow at $Re=22,000$ were first compared with available experimental and numerical results, and then the shear effects on Strouhal number and aerodynamic characteristics, and the underlying physical mechanism, were investigated. Time-averaged and unsteady flow patterns around the cylinder were studied to enhance understanding of the effects of velocity shear.

2. Computational model

2.1 Governing equations

The numerical model for the flow around a 5:1 rectangular cylinder was formulated using the Cartesian coordinate system. Eqs. (1) and (2) show the filtered continuity and Navier-Stokes equations for Large Eddy Simulation, in which the grid-scale turbulence is solved while the sub-grid-scale turbulence is modeled.

$$\frac{\partial \bar{u}_i}{\partial x_i} = 0 \tag{1}$$

$$\frac{\partial (\bar{u}_i)}{\partial t} + \frac{\partial (\bar{u}_i \bar{u}_j)}{\partial x_j} = -\frac{1}{\rho} \frac{\partial \bar{P}}{\partial x_i} + \frac{\partial}{\partial x_j} \left(\nu \frac{\partial \bar{u}_i}{\partial x_j} \right) - \frac{\partial \tau_{ij}}{\partial x_j} \tag{2}$$

where the over bar denotes the space filtered quantities. ρ , P and ν represent the air density, pressure and kinematic viscosity of the flow respectively. The subgrid scale stresses (SGS stress),

$\tau_{ij} = \overline{u_i u_j} - \overline{u_i} \overline{u_j}$, are expressed in Eq. (3)

$$\tau_{ij} - \frac{1}{3} \delta_{ij} \tau_{kk} = -2\nu_{SGS} \overline{S}_{ij} = \nu_{SGS} \left| \frac{\partial u_i}{\partial x_j} + \frac{\partial u_j}{\partial x_i} \right| \quad (3)$$

where ν_{SGS} is the SGS eddy viscosity

$$\nu_{SGS} = (C_S \overline{\Delta})^2 |\overline{S}| \quad (4)$$

where C_S is the Smagorinsky constant, which changes depending on the type of flow, and equals 0.1 in present study. $\overline{\Delta}$ is the size of the grid filter. $|\overline{S}| = [2\overline{S}_{ij}\overline{S}_{ij}]^{1/2}$ is the strain rate tensor.

2.2 Numerical approach

We studied the flow around the 5:1 rectangular cylinder by performing three-dimensional unsteady simulation of the incompressible governing equations shown above with the aid of the FLUENT package. The options offered by FLUENT[®] for simulation were carefully selected under the following considerations.

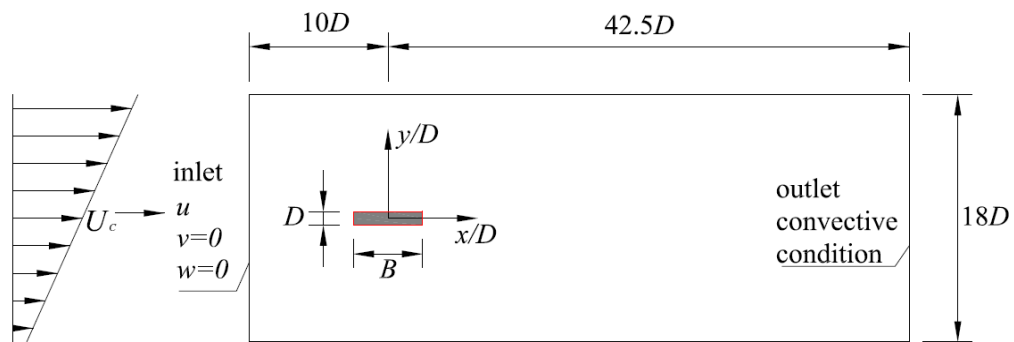
In the simulation, the velocity and the pressure are defined at the center of a control volume, while the volume fluxes are defined at the midpoint of their corresponding cell surfaces. In order to avoid oscillating problems, the Momentum Interpolation Method (MIM) developed by Rhie and Chow (1983) is used. The SIMPLE (Semi-Implicit Method for Pressure-Linked Equations) algorithm proposed by Patankar and Spalding (1972) was utilized, in which governing equations are solved sequentially because of their non-linearity and coupling characteristics and the solution loop is carried out iteratively in order to obtain a converged numerical solution. The pressure field is extracted by solving a pressure correction equation obtained by manipulating continuity and momentum equations, while the velocity field is obtained from the momentum equations. In addition, the convergence criterion of the iterative calculation was set to 1.0×10^{-6} , which required about 30 iterations to satisfy in the simulation.

In order to avoid instability caused by central-differencing schemes and non-physical wiggles, the bounded central differencing scheme is applied to spatial differencing of the convection term, which is a composite normalized variable diagram (NVD and Leonard 1991) scheme that consists of a pure central differencing, a blended scheme of the central differencing and the second-order upwind scheme, and the first-order upwind scheme. Meanwhile, a fully implicit second-order time-advancement scheme is chosen for temporal discretization to obtain stable and accurate simulation.

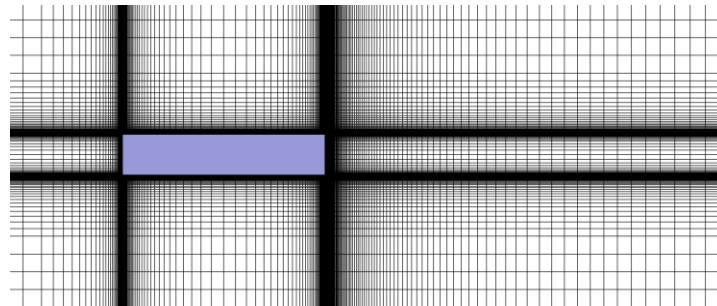
2.3 Discretisation and boundary conditions

As shown in Fig. 2(a), the computational domain was $52.5D$ in x -direction, $18D$ in y -direction and $5D$ in z -direction. The blockage ratio was 5.55%, which is smaller than the suggestion (6.4%) of Sohankar *et al.* (2000). The ratio of spanwise domain length L to chord length B was set to $L/B=1$ in order to achieve a good simulation of the mean and RMS of aerodynamic forces (Tamura

et al. 1998). L/B was also set to unity in the simulations of Mannini *et al.* (2010) and Bruno *et al.* (2010). A structured grid system of $325(x) \times 164(y) \times 24(z)$ is used to adequately resolve the flow (see Fig. 2(b)) with the first grid Δd near the body surface given empirically as $0.1/\sqrt{\text{Re}}$ ($\Delta d/D = 6.5 \times 10^{-4}$, $y^+ = 0.92$). For spatial discretization in the spanwise direction, 24 cells were uniformly distributed with a grid length $\Delta z/B = 0.042$, which is smaller than the minimum requirement $\Delta z/B = 0.1$ recommended by Tamura *et al.* (1998). The non-dimensional time-step, $\Delta t^* = \Delta t U/D$, was 5×10^{-3} , which maintained the Courant number $CL < 1$.



(a) Computational domain in x-y plane and boundary conditions



(b) Grid example near the cylinder

Fig. 2 Computer domain and grid example

The boundary conditions for simulation are as follows:

Body surface: A no-slip condition for $u_i = 0$ and a Neumann condition for pseudo-pressure ϕ are imposed.

Inlet: A UDF (User-Defined Function) condition, i.e., $U = U_c + Gy$, $v = 0$ and $w = 0$, and a Neumann condition of pseudo-pressure ϕ are imposed at the inlet boundary.

Outflow boundary: A convective boundary condition ($\partial\phi/\partial t + \bar{u} \cdot \partial\phi/\partial x = 0$) is applied for pseudo-pressure.

Spanwise: A periodic condition for velocity and pseudo-pressure is applied.

Upper and lower sides: A symmetric condition is applied.

3. Numerical results and discussions

3.1 Comparisons in non-shear flow

Table 1 compares the mean quantities that express the aerodynamics of the $B/D=5$ rectangular cylinder in non-shear flow obtained in the present and other studies. Both the mean drag coefficient C_D and Strouhal number St show good agreements. The reattachment length L_r , which is defined as the distance from the leading edge to the mean reattachment point, agrees reasonably well with those of other studies, especially Bruno *et al.* (2010). However, the fluctuating lift coefficient, C'_L , shows considerable deviation in all the studies including the present one, possibly because it is very dependent on the numerical methods and turbulence models.

Table 1 Mean quantities of 5:1 rectangular cylinder in non-shear flow. The averaging time T^* is defined as $T^*=tU/D$ where t is real flow time

Case	turbulence model	Re	St	C_D	C'_L	L_r/D	T^*
Ribeiro (2011)	URANS	40,000	--	1.170	0.90	--	--
Mannini <i>et al.</i> (2011)	DES-3D	26,400	0.103	1.029	0.421	4.750	464.5
Mannini <i>et al.</i> (2010)	LEA-3D	26,400	0.095	1.071	1.035	--	84.5
Mannini <i>et al.</i> (2010)	LEA-2D	26,400	0.094	1.060	1.075	4.650	74.2
Bruno <i>et al.</i> (2010)	LES-3D	40,000	0.115	1.060	0.75	4.665	550
Shimada and Ishihara(1998)	$k-\varepsilon$	22,000	0.118	1.010	0.05	--	--
Schewe (exp., 2009)	--	26,400	0.111	1.029	0.40	--	--
Matsumoto(exp., 2005) ^a	--	40,000	0.132	1.000	--	4.375	--
Present	LES-3D	22,000	0.118	1.100	0.89	4.632	250.0

^a extracted from Mannini *et al.* (2011)

Fig. 3 shows the time-averaged streamline of the flow field around the cylinder in non-shear flow ($\beta=0$), which is one of the most important items related to the aerodynamic characteristics of a rectangular cylinder. The flow separates at the sharp leading edge, reattaches to the side surface and re-separates at the trailing edge, with three vortices formed at different locations. The first vortex, with its core located at $\zeta/D=2.80$ ($\zeta=0$ denotes the leading edge of the rectangular cylinder), is the main vortex. Accompanying the first vortex, a secondary vortex is formed near the leading edge. Flow re-separation at the trailing edge creates the third vortex behind the cylinder. Fig. 3 shows asymmetry in the time-averaged flow between the two sides of the 5:1 cylinder. This

phenomenon of asymmetry in a symmetric setup has been reported and discussed by Bruno *et al.* (2012).

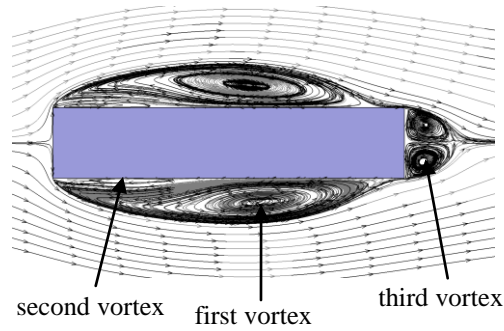


Fig. 3 Streamlines of the time-averaged flow field at $\beta=0$ around the cylinder

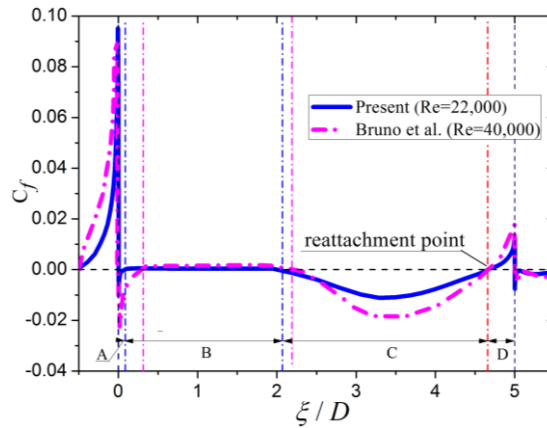


Fig. 4 Comparison of the distribution of the mean friction coefficient

The location of mean reattachment can be deduced from the distribution of the mean friction coefficient C_f , which is both time- and spanwise-averaged as for all the sectional quantities shown in this paper. Fig. 4 exhibits the distribution of C_f around the 5:1 rectangular cylinder, in which the regions of $-0.5 < \xi/D < 0$, $0 < \xi/D < 5$ and $5 < \xi/D < 5.5$ represent respectively the half leading surface, side surface and half trailing surface. The region of $0 < \xi/D < 5$ can be divided into four zones according to the sign (positive or negative) of C_f . In zones A and C, the mean friction coefficient is negative, which means the flow is reversing on average at the points near the side surface in these regions. The positive mean friction coefficients in Zones B and D correspond to forward flow. The point where C_f changes sign from negative to positive between Zones C and D is the reattachment point. As shown in Fig. 4, the mean reattachment point obtained in the present study appears at $\xi/D=4.632$, near the trailing edge. This result is almost the same as that of Bruno *et al.* (2010) with the value of $\xi/D=4.665$ at $Re=40,000$, and slightly larger than the

experimental result of Matsumoto *et al.* (2003) with $\xi/D = 4.375$ at $Re=20000$, and slightly smaller than that of Mannini *et al.* (2011) with $\xi/D = 4.75$ in their DES simulation at $Re=26,400$. On the other hand, it is also seen in Fig. 4 that there is considerable difference in the distribution of C_f along the cylinder, although the present simulation creates a reattachment point similar to that of Bruno *et al.* (2010). Although Reynolds number no doubt plays some roles in determining the reattachment point in the discussed Reynolds number region, it may be reasonable to conclude that the large scale vortex structure is not so sensitive to the turbulence model or numerical method that it can be comparatively easily captured.

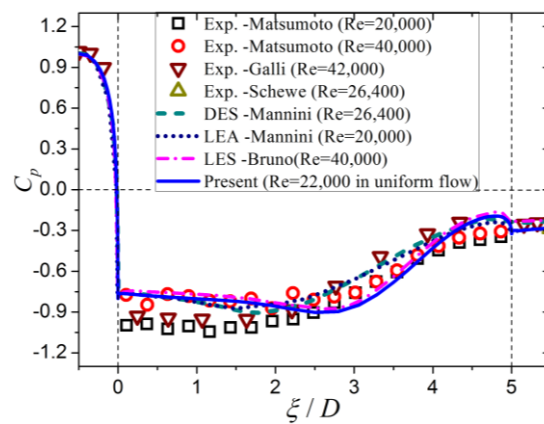


Fig. 5 Comparison of the distribution of mean pressure coefficient over the rectangular cylinder surface in non-shear flow

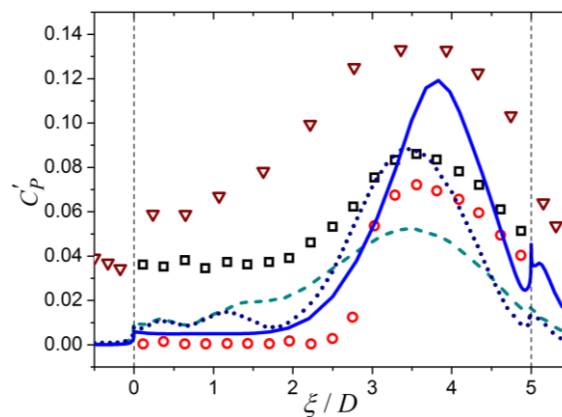


Fig. 6 Comparison of the distribution of t-std pressure coefficient over the rectangular cylinder surface in non-shear flow (symbols as in Fig. 5).

Fig. 5 shows the distributions of the mean pressure coefficient C_p on the 5:1 rectangular

cylinder surface. The pressure coefficient C_p is defined as $C_p = (P - P_\infty)/(0.5\rho U_C^2)$, where P is the local mean pressure on the cylinder surface and P_∞ is the pressure upstream of the cylinder.

The experimental results obtained by Matsumoto and Galli are extracted from Mannini *et al.* (2011). The distribution of the mean pressure coefficient C_p of the present study agrees reasonably well with other numerical and experimental results, although the deviation between the experimental and numerical results of region $0 < \xi/D < 2$ were not improved either in the present study. On the back surface of the rectangular cylinder ($5 < \xi/D < 5.5$), the base pressure coefficient of the present results is the minimum of the summarized studies, resulting in the maximum mean drag coefficient in Table 1. For the fluctuating pressure coefficient C'_p , an obvious scatter among the reported studies including the present simulation can be seen in Fig. 6. The instantaneous pressure is so sensitive to the numerical methods, turbulence model, Reynolds number, and the turbulence intensity level of the nominal uniform flow of an experiment that it is very difficult to obtain the same result for C'_p in different studies. Even so, all the curves shown in Fig. 6 exhibit peak values of C'_p at a location around $\xi/D \approx 3.75$, which supports the conclusion of Matsumoto *et al.* (2003) that the location of maximum C'_p is strongly correlated with the mean reattachment point. Meanwhile, the scatter of C'_p inevitably creates a difference in fluctuating lift coefficient C'_L . As summarized in Table 1, C'_L varies from 0.40 to 1.075 in the reported numerical and experimental results including that in the present study ($C'_L = 0.89$).

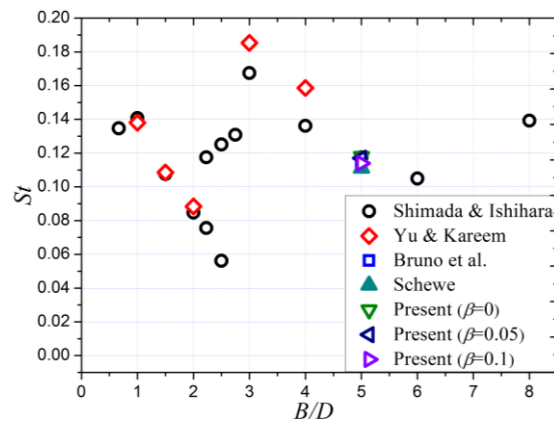


Fig. 7 Comparison of Strouhal number with literatures

3.2 Vortex shedding in shear flow

The Strouhal number $St=fD/U$ is calculated from the FFT analysis of the lift coefficient of the 5:1 rectangular cylinder in non-shear and shear flows at $Re=22,000$, where f is the dominant vortex shedding frequency. The result obtained in the present study is $St=0.118$ at $\beta=0$, $St=0.117$ at $\beta=0.05$ and $St=0.118$ at $\beta=0.1$, which is almost unchanged with the shear parameter. In addition, the Strouhal number obtained in non-shear flow is compared with those obtained in other studies in

Fig. 7, which exhibits the variation of Strouhal number with side ratio. The present result, $St=0.118$ in non-shear flow, is very close to the numerical results of Yu and Kareem (1996) with $St=0.114$, Bruno *et al.* (2010) with $St=0.115$, and the experimental result of Schewe (2009) with $St=0.111$. Meanwhile, Fig. 7 shows that the Strouhal number depends strongly on the side ratio.

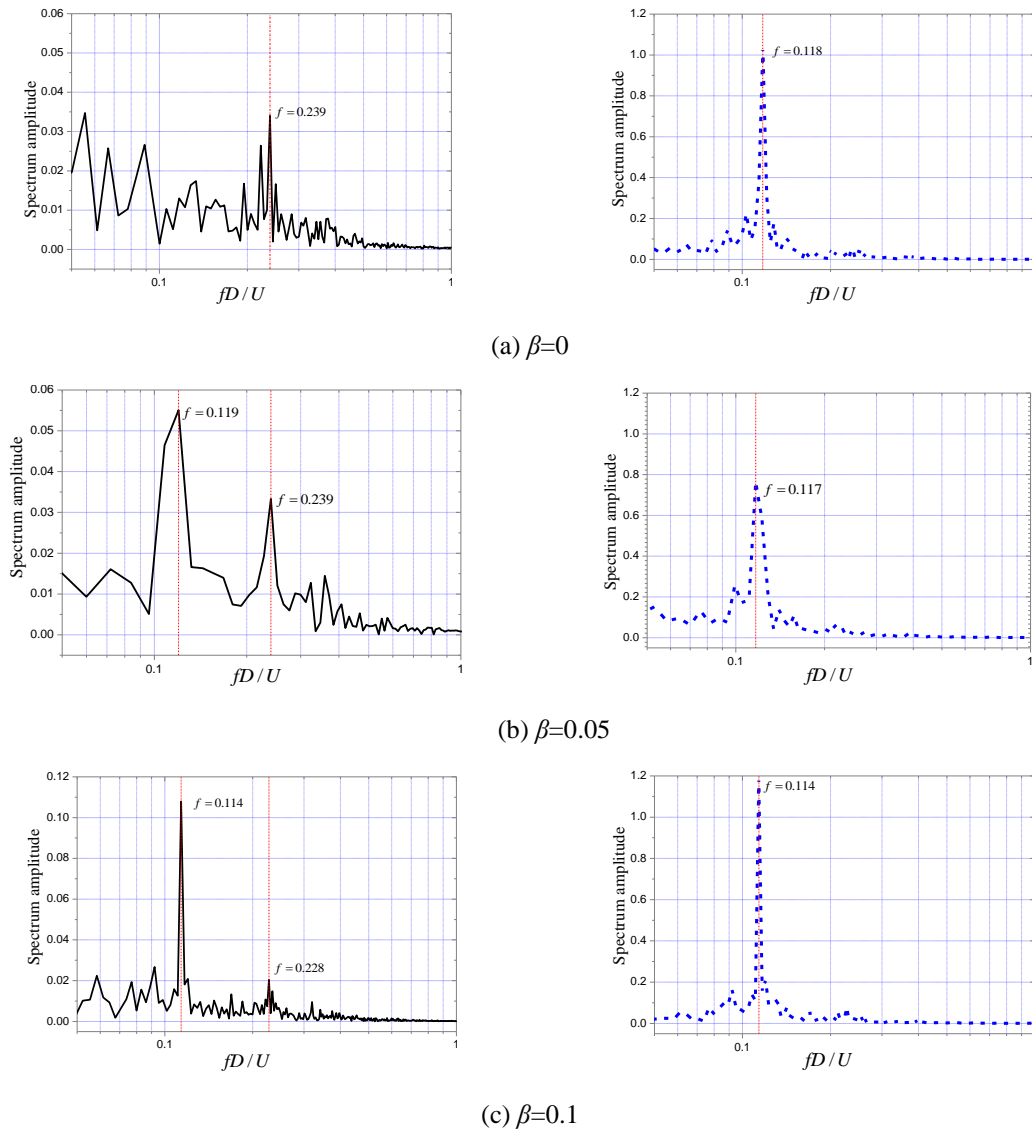


Fig. 8 Spectra of drag and lift coefficients with different shear parameters (left: drag; right:lift)

Discontinuities or uncertainties of the Strouhal number exist at around $B/D=2.8$, resulting from the delicate intermittent reattachment of the separated shear layer. The separated flow does not

reattach to the side surface when $B/D < 2.8$, fully reattaches when $B/D > 6$, and intermittently reattaches in the range of $2.8 < B/D < 6$. The $B/D=5$ section of the present study belongs to the intermittent reattachment range. The result that Strouhal number does not vary significantly with shear parameter was also observed for rectangular cylinders with $B/D=0.2-3$ by Onitsuka *et al.* (2000) in their experiment. It seems reasonable to conclude that the shear parameter does not bring significant change to the Strouhal number of rectangular cylinders, although it creates asymmetry into the wake structure as shown later.

Fig. 8 compares the power spectra of the instantaneous drag and lift coefficients of the 5:1 rectangular cylinder for different shear parameters ($\beta=0, 0.05$ and 0.1) at $Re=22,000$. The solid line shows the spectrum of drag coefficient C_D and the broken line shows that of lift coefficient C_L . In non-shear flow, there is only one peak each in the power spectra of lift and drag coefficients, and the peak frequency of fluctuation of C_D is approximately twice that of C_L , as shown in Fig. 8(a).

For the shear flow, although the fluctuating lift coefficient still has one harmonic like that for $\beta=0$, a subharmonic has entered into the fluctuation of C_D . The strength of the subharmonic increases as the shear rate increases and it becomes dominant, resulting in the peak fluctuation frequencies of C_L and C_D becoming identical at $\beta=0.1$. A similar phenomenon was also reported for a square cylinder (Cao *et al.* 2012).

The behaviour of the power spectrum shown in Fig. 8 is related to the wake pattern behind the rectangular cylinder. Fig. 9 shows the variation of time-averaged streamlines at the near wake with different shear parameters. It is obvious that there are two dominate vortices at $\beta=0$, two asymmetric vortices at $\beta=0.05$ and only one dominant vortex at $\beta=0.1$. With the increase in shear parameter, the time-averaged vortices at the high velocity side gradually decayed and almost disappeared at $\beta=0.1$, which implies that they no longer alternatively shed from the two sides of the cylinder in shear flow.

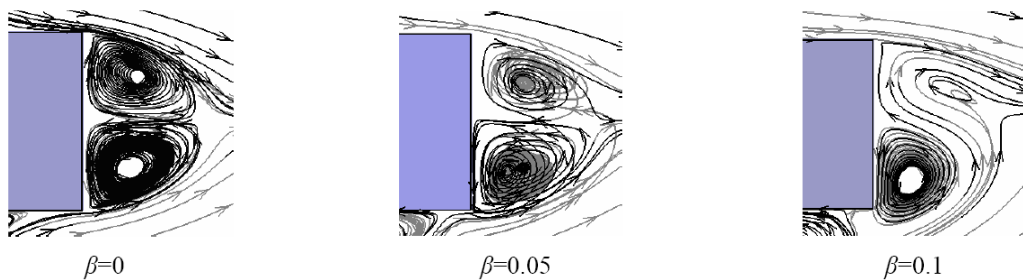


Fig. 9 Streamlines of the time-averaged flow field behind the rectangular cylinder

Fig. 10 compares the instantaneous iso-vorticity surface of the primary Karman vortex between no-shear and shear flows, where the dashed and solid lines represent clockwise and counterclockwise vortices, respectively. All the figures correspond to the moment when the lift coefficient is maximum. The vortices appear alternatively in the wake when $\beta=0$. However, with an increase in shear parameter, the counterclockwise vortices on the low-velocity side become weaker and disappear in the far wake at $\beta=0.1$. The Karman vortex street is broken, but the counterclockwise vortex on the low-velocity side still exists in the near wake, and vortex shedding never disappears. This complicated flow structure in the wake is very important when considering

the environmental disturbance downstream of a large structure.

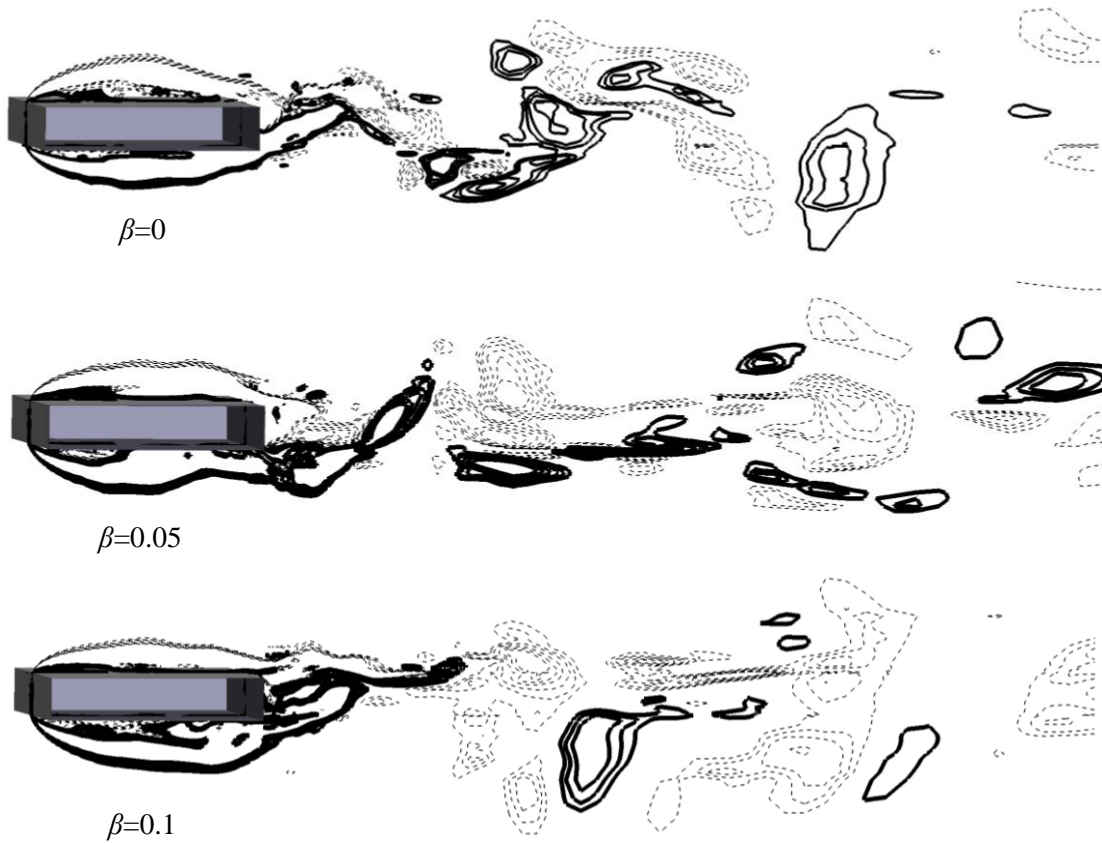


Fig. 10 Instantaneous wake structure with different shear parameters, $\omega_z = \pm 2$

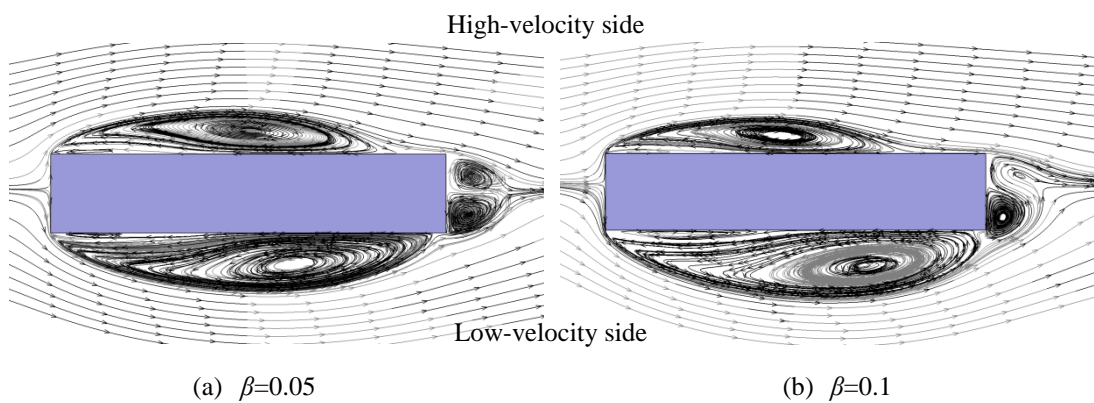


Fig. 11 Streamlines of the time-averaged flow field around the cylinder

3.3 Aerodynamic forces in shear flow

The time-averaged streamlines of flow field around the rectangular cylinder with different shear parameters are compared in Fig. 11. The first and second vortex can be observed on both the upper and lower surfaces in shear flow, although they are no longer symmetric as in non-shear flow. With the increase in the shear parameter, the centre position of the first vortex (separation bubble) moves upstream on the high-velocity side, and downstream on the low-velocity side. However, the separation bubble on the high-velocity side becomes thinner while its counterpart on the low-velocity side becomes thicker. The mean recirculation region forming after the trailing edge in non-shear flow on the high velocity side disappears when $\beta=0.1$. These complicated flow phenomena directly influence the aerodynamic forces on the 5:1 rectangular cylinder.

Table 2 Intermittency factor of positive forward flow at different positions at trailing edge

shear parameter	position: y/D	Point-1	Point-2	Point-3	Point-4
		± 0.5005	± 0.5050	± 0.5100	± 0.6500
$\beta=0$	Low-velocity side	72.5%	74.5%	74.8%	90.6%
	High-velocity side	71.1%	72.1%	73.6%	90.9%
$\beta=0.05$	Low-velocity side	53.3%	56.3%	56.4%	59.7%
	High-velocity side	88.9%	90.1%	90.8%	97.8%
$\beta=0.1$	Low-velocity side	46.9%	48.6%	47.8%	49.7%
	High-velocity side	90.2%	92.5%	94.1%	100.0%

Here we illustrate the variation of the unsteady dynamic flow structure around the 5:1 rectangular cylinder with shear parameter by showing quantitatively the change of intermittency factor of flow reattachment, which is defined as the fraction of time during which the flow at the trailing edge is not reversal, i.e., the flow is completely forward when intermittency factor equals 1, or completely reversal when the intermittency factor equals 0. The streamwise velocity is monitored at 8 points located at $y/D=\pm 0.5005$, ± 0.5050 , ± 0.5100 and ± 0.6500 at the trailing edge, as shown in Fig. 1. The variation of intermittency factor with shear parameter is shown in Table 2.

At $\beta=0$ (non-shear flow), the intermittency factor has a similar value, but not equal to 0 or 1, on the upper and lower sides of the cylinder, implying that the separated layer reattaches intermittently and almost symmetrically on the side surfaces. However, with the increase in shear parameter, the intermittency factor becomes greater on the high-velocity side and smaller on the low-velocity side, which means the intermittently reattached flow becomes more stably reattached on the high-velocity side and more stably separated on the low-velocity side. Fig. 12 compares the mean friction coefficient C_f distributions around the rectangular cylinder for shear and non-shear flows. The distribution of mean friction coefficient distribution becomes asymmetrical in the shear flow. With the increase in the shear parameter, the mean reattachment length L_r decreases from $L_r/D=4.632$ ($\beta=0$) to $L_r/D=4.469$ ($\beta=0.05$) and $L_r/D=4.073$ ($\beta=0.1$) on the-high velocity side, while it increases from $L_r/D=4.632$ ($\beta=0$) to $L_r/D=4.850$ ($\beta=0.05$) and $L_r/D=4.868$ ($\beta=0.1$) on

the low-velocity side, which means upstream and downstream movement of the separation bubble on the high- and low-velocity sides, respectively.

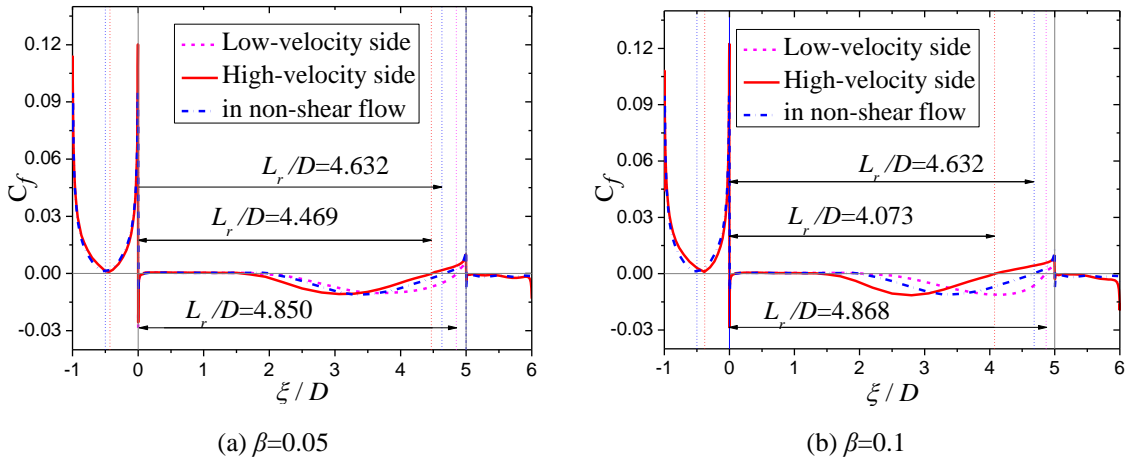


Fig. 12 Comparison of the distribution of the mean friction coefficient in shear flow and non-shear flow

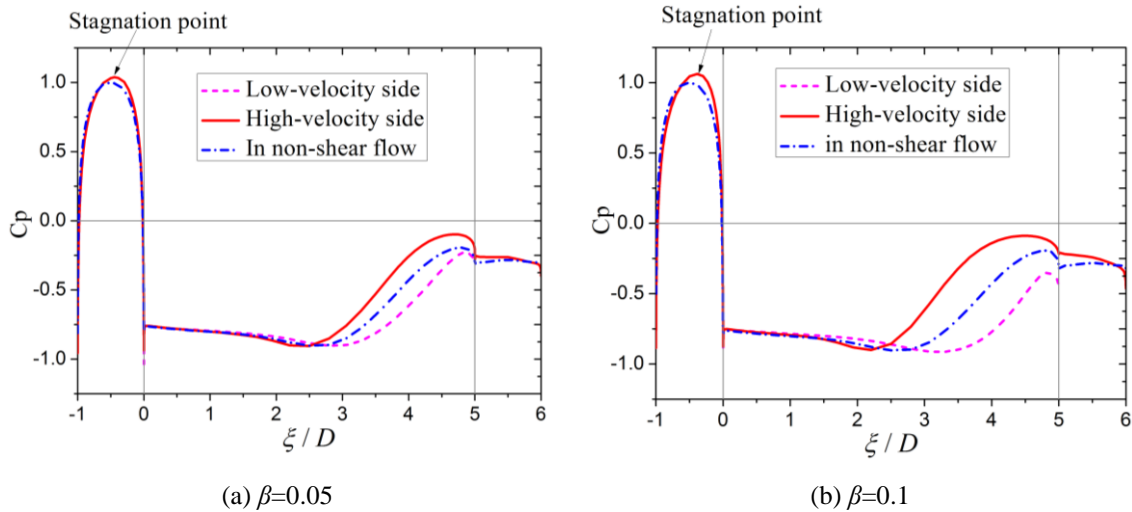


Fig. 13 Comparison of mean pressure coefficient over the rectangular cylinder in non-shear and shear flows

Fig. 13 compares the mean pressure coefficient distribution around the rectangular cylinder in non-shear and shear flows. By comparison in the region of $-1 < \xi/D < 0$ (front surface), it can be observed that the stagnation point moves to the high-velocity side in shear flows. The movement of the stagnation point with shear parameter is shown in Fig. 14, where the stagnation angle θ is defined as the angle of the stagnation point to the cylinder center, as illustrated in Fig. 1. In the

non-shear flow, the stagnation point is at the center and the angle θ is equal to zero ($\theta=0$). With the increase of the shear parameter, the stagnation point angle increases almost linearly. The movement of the stagnation point with shear parameter for circular and square cylinders found by one of the authors of the present study is also shown in Fig. 14, which implies that the movement of the stagnation point to the high velocity side is an inherent phenomenon in shear flow.

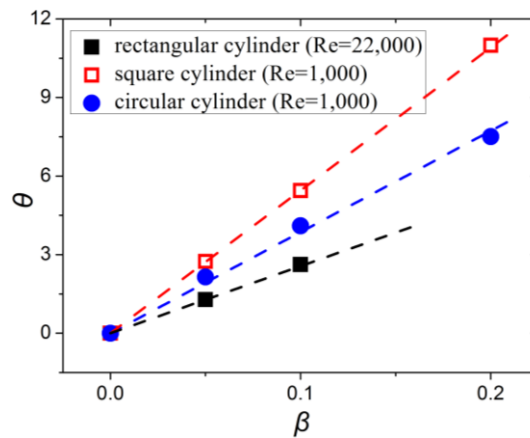


Fig. 14 Movement of the stagnation point with shear parameter for different cross section cylinders. The data for the square and circular cylinders is from the ref. Cao *et al.* (2012) and Cao *et al.* (2010)

As shown in Fig. 13, the mean pressure coefficients on the upper and lower surfaces in shear flows are almost the same in the region of $0 < \xi/D < 2.5$, but exhibit significant difference near the region of $2.5 < \xi/D < 5$, and this difference increases with increase in shear parameter, which can be seen by comparison between Figs.13(a) and 13(b). This difference is directly related to the asymmetrically located separation bubbles on the upper and lower surfaces, which move upstream and downstream on the high- and low-velocity sides, respectively.

For the region of $5 < \xi/D < 6$ (trailing side), the absolute value of mean base pressure coefficient decreases with increase in shear parameter. This is similar to the experimental result of Onitsuka *et al.* (2000), which reported that the base pressure of a rectangular cylinder with $B/D=0.1-3.0$ recovered slightly in shear flows.

The asymmetric pressure distribution and particular flow pattern in shear flow lead to different aerodynamic forces on the 5:1 rectangular cylinder in shear flow. Fig. 15 illustrates examples of time histories of the drag and lift coefficients in shear flow, which exhibit stochastic characteristics. Table 3 summarizes the variation of mean and fluctuating drag, lift and moment coefficients with shear parameter. The mean drag coefficient, which is the summation of pressure and friction forces, increased slightly (less than 4%) compared with that in non-shear flow in the investigated shear parameter region. The higher pressure field on the high-velocity side and lower pressure field on the low-velocity side results in a downward lift force towards the low-velocity side, and the mean lift coefficient increases with increase in shear parameter, as shown in Fig. 16. Meanwhile, the moment coefficient is no longer zero in shear flow. A negative moment force is found due to the asymmetric pressure distribution, and its magnitude also increases with increase in shear parameter.

Fig. 16 shows the variation of fluctuating drag, lift and moment coefficient with shear parameter. All three fluctuating force coefficients also increase almost linearly with increase in shear parameter.

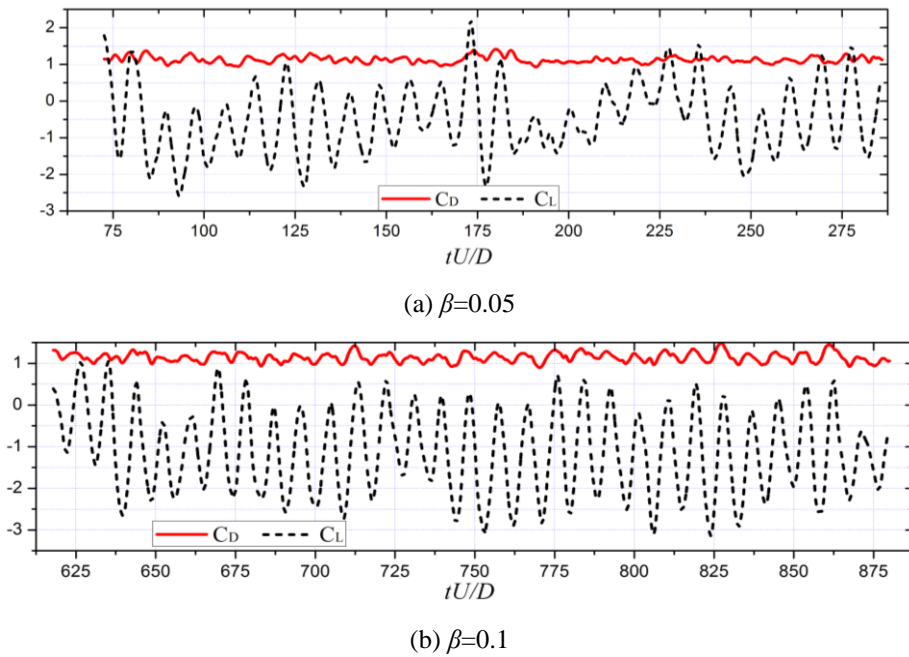


Fig. 15 Time histories of the drag and lift coefficients in shear flows

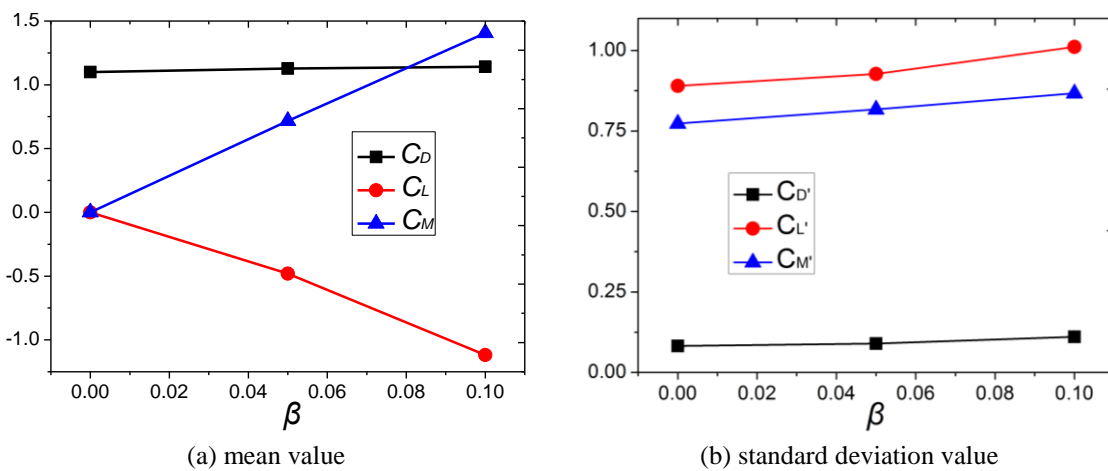


Fig. 16 Variation of the force on the rectangular cylinder with shear parameter

Table 3 Comparison of mean and standard deviation values of aerodynamic force coefficients (normalized with respect to body thickness D) with different shear parameters

Shear parameter	C_D	C_D'	C_L	C_L'	C_M	C_M'	T^*
$\beta=0$	1.100	0.082	--	0.890	--	0.773	279.5
$\beta=0.05$	1.128	0.090	-0.480	0.927	0.717	0.817	213.4
$\beta=0.1$	1.142	0.111	-1.119	1.011	1.405	0.867	262.1

Interestingly, the direction of the lift force on the 5:1 rectangular cylinder is the same as that on a circular cylinder, but opposite to that on a square cylinder. One of the authors of this study suggested that the aerodynamic characteristics of a bluff body in shear flow received the combined effects of the movements of stagnation point, separation point and reattachment points if it exists (Cao *et al.* 2010, 2012). For a circular cylinder, the contribution of the movement of stagnation point is dominant, which leads to a lift force from high- to low-velocity side. For the cases of a square and a 5:1 rectangular cylinder, the movement of stagnation point does not contribute directly to the lift force. Furthermore, the separation point is fixed at the sharp leading edge, but the flow separates without reattachment for the square cylinder while there is intermittent flow reattachment for the 5:1 rectangular cylinder. The pressure is generally low on the high-velocity side and high on the low-velocity side of a square cylinder, in which the flow is fully separated, thus creating a positive lift force towards the high-velocity side. However, for the 5:1 rectangular cylinder, the intermittent reattachment behavior becomes more stably reattached on the high-velocity side and more stably separated on the low-velocity side. The separation bubble moves upstream and downstream on the high- and low-velocity sides respectively, and creates negative lift and positive moment forces in shear flow.

4. Conclusions

This paper has described a numerical simulation to investigate the aerodynamic characteristics of a 5:1 rectangular cylinder in both non-shear and shear flows at a Reynolds number of $Re=22,000$. Particular attention was devoted to the effects of velocity shear in the oncoming flow. Time-averaged and unsteady flow patterns around the cylinder were studied to enhance understanding of the effects of velocity shear. Conclusions are as follows.

The Strouhal number has no significant variation with oncoming velocity shear, while the peak fluctuation frequency of the drag coefficient becomes identical to that of the lift coefficient with increase in velocity shear. The Karman vortex street is broken in shear flow.

The stagnation point moves to the high-velocity side, and the stagnation angle increases almost linearly with increasing shear parameter.

The intermittently-reattached flow that is a feature of the aerodynamics of the 5:1 rectangular cylinder in uniform flow, becomes more stably reattached on the high-velocity side, and more stably separated on the low-velocity side in shear flow. The separation bubble moves upstream and downstream at the high- and low-velocity sides in shear flow, respectively.

In the range of shear parameter at $Re=22,000$ investigated, the mean drag coefficient increases slightly with increase in velocity shear. The mean lift and moment coefficients increase almost

linearly with velocity shear. All three fluctuating force coefficients increase with increase in shear parameter. The lift force acts from the high-velocity side to low-velocity side, which is similar to that of a circular cylinder but opposite to that of a square cylinder under the same oncoming shear flow conditions.

Acknowledgments

This research was funded in part by the Natural Science Foundation of China (NSFC) Grant No. 50978202, Shanghai Pujiang Program number 10PJ1409700 and SLDRCE09-B-04.

References

- Bartoli, G., Bruno, L., Buresti, G., Ricciarelli, F., Salvetti, M.V. and Zasso, A. (2008), *BARC overview document*, <http://www.aniv-iawe.org/barc>.
- Bartoli, G., Borsani, A., Mannini, C., Marra, A.M., Procino, L. and Ricciardelli, F. (2011), "Wind tunnel study on the aerodynamics of a 5:1 rectangular cylinder in smooth flow", *Proceedings of the 13th International Conference on Wind Engineering*, Amsterdam, Netherlands.
- Bronkhorst, A.J., Geurts, C.P.W. and van Bentum, C.A. (2011), "Unsteady pressure measurements on a 5:1 rectangular cylinder", *Proceedings of the 13th International Conference on Wind Engineering*, Amsterdam, Netherlands.
- Bruno, L., Fransos, D., Coste, N. and Bosco, A. (2010), "3D flow around a rectangular cylinder: A computational study", *J. Wind Eng. Ind. Aerod.*, **98**(6-7), 263-276.
- Bruno, L., Coste, N. and Fransos, D. (2012), "Simulated flow around a rectangular 5:1 cylinder: Spanwise discretisation effects and emerging flow features", *J. Wind Eng. Ind. Aerod.*, **104-106**, 203-215.
- Cao, S.Y., Ozono, S., Tamura, Y., Ge, Y.J. and Kikugawa, H. (2010), "Numerical simulation of Reynolds number effects on velocity shear flow around a circular cylinder", *J. Fluids Struct.*, **26**(5), 685-702.
- Cao, S.Y., Ge, Y.J. and Tamura, Y. (2012), "Shear effects on flow past a square cylinder at moderate Reynolds numbers", *J. Eng. Mech. - ASCE*, **138**(1), 116-123.
- Kiya, M., Tamura, H. and Arie, M. (1980), "Vortex shedding from a circular cylinder in moderate Reynolds number shear flow", *J. Fluid Mech.*, **101**(4), 721-735.
- Le, T., Matsumoto, M. and Shirato, H. (2009), "Spanwise coherent structure of wind turbulence and induced pressure on rectangular cylinders", *Wind Struct.*, **2**(5), 441-455.
- Leonard, B.P. (1991), "The Ultimate conservative difference scheme applied to unsteady one-dimensional advection", *Computer Method. Appl. M.*, **88**(1), 17-74.
- Mannini, C., Soda, A. and Schewe, G. (2010), "Unsteady RANS modelling of flow past a rectangular cylinder: Investigation of Reynolds number effects", *Comput. Fluids.*, **39**(9), 1609-1624.
- Mannini, C., Soda, A. and Schewe, G. (2011), "Numerical investigation on the three-dimensional unsteady flow past a 5:1 rectangular cylinder", *J. Wind Eng. Ind. Aerod.*, **99**(4), 469-482.
- Matsumoto, M. (1996), "Aerodynamic damping of prisms", *J. Wind Eng. Ind. Aerod.*, **59**(2-3), 159-175.
- Matsumoto, M., Shirato, H., Araki, K., Haramura, T. and Hashimoto, T. (2003), "Spanwise coherence characteristics of surface pressure field on 2-D bluff bodies", *J. Wind Eng. Ind. Aerod.*, **91**(1-2), 155-163.
- Norberg, C. (1993), "Flow around rectangular cylinders: pressure forces and wake frequencies", *J. Wind Eng. Ind. Aerod.*, **49**(1-3), 187-196.
- Ong, L. and Wallace, J. (1996), "The velocity field of the turbulent very near wake of a circular cylinder", *Exp. Fluids.*, **20**(6), 441-453.
- Onitsuka, S., Ozono, S., Cao, S. and Wakasugi, Y. (2000), "Flow around rectangular cylinders in linear shear flow", *Proceedings of the 16th Japanese National Wind Engineering Symp.*, Tokyo.

- Patankar, S.V. and Spalding, D.B. (1972), "A calculation procedure for heat, mass and momentum transfer in three-dimensional parabolic flows", *Int. J. Heat Mass. Tran.*, **15**, 1787-1806.
- Ribeiro, A.F.P. (2011), "Unsteady RANS modelling of flow past a rectangular 5:1 cylinder: investigation of edge sharpness effects", *Proceedings of the 13th International Conference on Wind Engineering*, Amsterdam, Netherlands.
- Schewe, G. (2009), "Reynolds-number-effects in flow around a rectangular cylinder with aspect ratio 1:5", *Proceedings of the 50th European and African Conference on Wind Engineering*, Florence, Italy.
- Shimada, K. and Ishihara, T. (2002), "Application of a modified k-epsilon model to the prediction of aerodynamic characteristics of rectangular cross-section cylinders", *J. Fluid. Struct.*, **16**(4), 465-485.
- Smagorinsky, J. (1963), "General circulation experiments with the primitive equations", *Mon. Weather Rev.*, **91**, 99-164.
- Sohankar, A., Davidson, L. and Norberg, C. (2000), "Large eddy simulation of flow past a square cylinder: Comparison of different subgrid scale models", *J. Fluid. Eng.- T. ASME*, **122**(1), 39-47.
- Sumner, D. and Akosile, O.O. (2003), "On uniform planar shear flow around a circular cylinder at subcritical Reynolds number", *J. Fluid. Struct.*, **18**(3-4), 441-454.
- Tamura, T., Miyagi, T. and Kitagishi, T. (1998), "Numerical prediction of unsteady pressures on a square cylinder with various corner shapes", *J. Wind Eng. Ind. Aerod.*, **74-76**, 531-542.
- Yu, D. and Kareem, A. (1996), "Two-dimensional simulation of flow around rectangular prism", *J. Wind Eng. Ind. Aerod.*, **62**(2-3), 131-161.